Detecting methane emissions from palm oil mills with airborne and spaceborne imaging spectrometers

Adriana Valverde[1*], Javier Roger[1], Javier Gorroño[1], Itziar Irakulis-Loitxate[2,1] and Luis Guanter[1,3]

[1] Research Institute of Water and Environmental Engineering (IIAMA), Universitat Politècnica de València, Spain.

[2] International Methane Emission Observatory (IMEO), United Nations Environment Programme, Paris, France.

[3] Environmental Defense Fund, Amsterdam, Netherlands.

* Corresponding author's email: avaligl@doctor.upv.es

Abstract

Methane (CH_4) emissions from human activities are a major cause of global warming, necessitating effective mitigation strategies. In particular, the palm oil industry generates palm oil mill effluent (POME), which continuously emits methane into the atmosphere. Satellites are becoming a powerful tool to detect and quantify methane emissions, but there is no evidence of their ability to monitor those from palm oil mill ponds. In this work, we have tested the potential of methane-capable satellite instruments to detect and quantify emissions from these ponds. We have focused on the satellite missions with the highest sensitivity to methane emissions, namely the GHGSat commercial constellation and the PRISMA, EnMAP, and EMIT imaging spectroscopy missions. We have also tested the AVIRIS-NG airborne imaging spectrometer. We report three methane plumes from palm oil mills in Indonesia with GHGSat and two in Colombia with AVIRIS-NG. In the cases of EnMAP, PRISMA and EMIT, we observed substantial methane concentration enhancements over several ponds in Indonesia, Malaysia, and Colombia. It remains unclear whether they are due to retrieval artifacts caused by the particular albedo of the ponds, although the low spatial correlation between those enhancements and the ponds suggests that at least a fraction of the enhancements is caused by real emissions. By leveraging advanced imaging techniques and satellite data, this research contributes to progressing strategies to address new methane emissions sources with high mitigation potential, providing a first step toward the satellite-based monitoring of methane emissions from palm oil mills.

Introduction

Methane (CH_4) is a potent greenhouse gas (GHG) and the second most significant anthropogenic contributor to global warming after carbon dioxide (CO_2). Since pre-industrial times, methane has been responsible for about 0.6 °C rise in global temperatures, as methane has a warming potential about 80 times greater than CO_2 over a 20-year period[1]. With a relatively short atmospheric lifetime of around nine years, mitigating anthropogenic methane emissions is considered the fastest and most effective strategy to combat global warming in the short to medium term. Methane is emitted by diverse anthropogenic sources, including livestock, oil and gas systems, coal mining, landfills, wastewater treatment, and agriculture. In particular, the waste industry is the third largest contributor, accounting for about 19% of anthropogenic emissions. Palm oil production constitutes a portion of wastewater emissions, and wastewater contributes ~ 8% of total waste emissions[2].

In the oils and fats industry, palm oil plays a central role and is vital in the socioeconomic development of the countries where it is produced[3]. In the past two decades, oil palm plantations have covered more than 21 million hectares, deeply impacting natural forest ecosystems and contributing directly to climate change by releasing carbon from converted forests and peatlands into the atmosphere[4]. According to the United States Department of Agriculture[5], global palm oil production in 2023 reached 79.46 million metric tons. Fig. 1 depicts palm oil production by country in 2023, with Indonesia leading as the largest producer at 47 million tons (59% of global production) with currently 1,231 palm oil mills (POMs), as reported by the Universal Mill List (UML)[6].
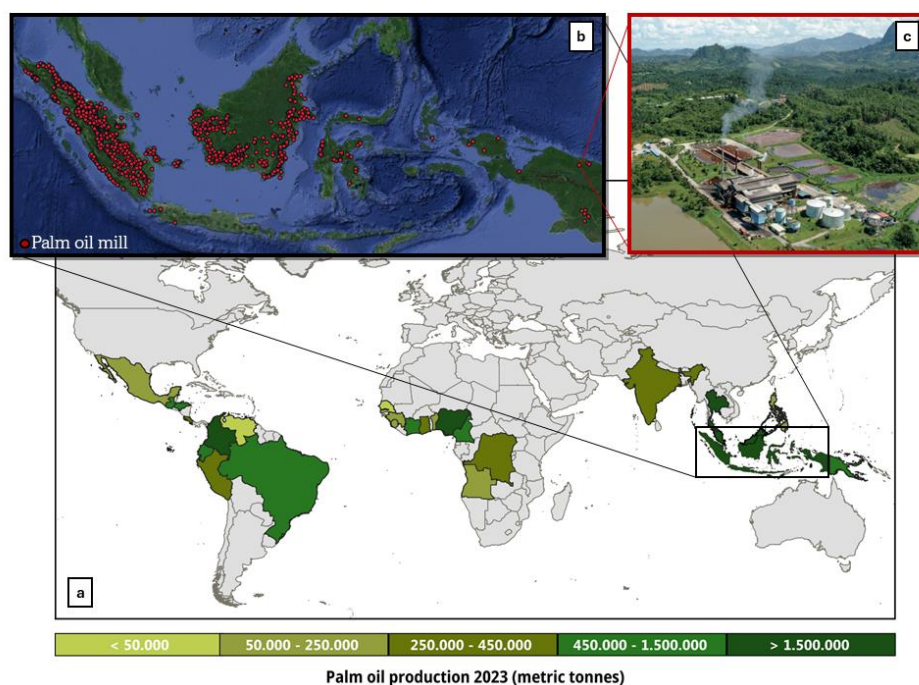
Figure 1. Global distribution of palm oil production and processing facilities. a) Palm oil production in 2023 (Data source: US Department of Agriculture[5]). b) Location of POMs in Indonesia (Data source: UML[6]. Map background: Google Earth). C) Typical POM in Indonesia (Image source: Viridis Engineering[7]).

Palm oil is extracted from the mesocarp of palm tree fruits (*Elaeis guineensis* Jacq.), while palm kernel oil (PKO) is obtained from the kernel[8]. During palm oil production, palm oil mill effluent (POME) is generated through the sterilization of fresh fruit bunches (FFB), the clarification of extracted crude palm oil (CPO), hydrocyclone operations, and the separation of kernel and shell[9]. POME, characterized by its brown colour, contains ~95% water, ~4-5% suspended organic matter and particulate matter, and ~0.6% oil. These properties (Table S1), combined with an acidic pH of 4.5 and an average temperature of 80-90ºC, contribute to its high levels of chemical oxygen demand (COD) and biochemical oxygen demand (BOD), which require pre-treatment before discharge into the environment[10].

Most POMs have adopted the conventional ponding system for POME treatment, which consists of a series of open ponds: de-oiling tank, cooling ponds, acidification ponds, anaerobic ponds, facultative ponds or aerobic ponds. During anaerobic digestion in the ponds, anaerobic bacteria degrade complex organic materials without oxygen through various reactions such as hydrolysis, acidogenesis (including acetogenesis), and methanogenesis, resulting in methane, carbon dioxide, and water. The proportion of methane and carbon dioxide emitted to the atmosphere from these anaerobic open ponds is approximately 60% methane and 40% carbon dioxide[11-12]. For this reason, many POMs install biodigesters to effectively capture biogas from anaerobic digestion to generate energy, reducing GHG emissions by approximately 75% per tonne of CPO produced[13]. Additionally, this biogas system represents a substantial economic and energy source for the countries, generating about 1.8 kWh for every 1 m^3 of biogas. Although the characteristics of the POME determine the electrical energy conversion achieved, it is estimated that this energy generation represents approximately 25% energy conversion efficiency, with the remainder being lost as heat[14]. POME has a higher biomethane emission rate than other feedstocks like manure, biomass, and municipal waste, highlighting its considerable potential for renewable energy generation. Besides, biogas upgrading offers additional benefits, including zero waste management and fertilizer production[15]. However, three of the largest palm oil producers (Indonesia[16], Malaysia[3], and Colombia[17]) have less than 10, 30, and 12% of their mills with biogas systems, respectively, releasing large quantities of methane directly into the atmosphere.

Some previous on-site studies have provided approximate values for methane emissions in anaerobic ponds. For example, studies conducted by Enström *et al.*[18] and Yacob *et al.*[19] have used different static collection chambers on the surface of ponds to capture methane flux and reported an averaging 315 kg/h and 114 kg/h of methane per pond, respectively. Other studies estimate that the methane emission rate from the ponds is 6.54 kg/t FFB (Schuchardt *et al.*[20]), which in a mill with a processing capacity of 30-45 t FFB/h would result in methane emissions of between 196-294 kg/h per pond. Additionally, Conil *et al.*[21] presented data from several POMs reporting their methane production, where the average for these facilities is 8-11 kg CH_4/t FFB, which, following the previous example, would correspond with emissions between 240-330 kg/h. However, considering the maximum of these mills of around 15 kg CH_4/t FFB, these emissions could reach 675 kg/h. Nevertheless, these emissions are not constant and are affected by the seasonal cultivation of oil palm, the number of ponds, and the activities of each mill. Even

so, extrapolating these findings to real cases with variable pond sizes and conditions suggests that typical methane emission rates might range from 100-450 kg/h/pond.

Improved methodologies and the high-resolution satellite data becoming available in recent years are increasing methane detection capabilities and revealing new sources from space. The 100-450 kg/h range of methane emission rates expected from POME is comparable to the detection limit of satellite-based imaging spectrometers currently used to detect and quantify methane plumes from point sources. High-resolution hyperspectral satellites, such as the GHGSat constellation or the PRISMA, EnMAP, and EMIT scientific missions, have demonstrated a great ability to detect anthropogenic methane emissions such as oil and gas extraction, landfills, and coal mining. The detection limits of these instruments under the best conditions are about 500 kg/h for PRISMA, EnMAP and EMIT[22-25], and ~100 kg/h for GHGSat instrument[26]. On the other hand, airborne campaigns with imaging spectrometer instruments, such as AVIRIS-NG, have shown great potential for detecting methane point sources, with a detection limit that can be as low as 10 kg/h thanks to the high spatial sampling and the good spectral and radiometric performance[27].

This work focuses on assessing the ability of these instruments to detect methane emissions from POMs, a challenge for satellite sensors due to the combination of weak and spatially distributed emissions with low surface reflectance and high scene heterogeneity. We consider this study as an initial step to explore these new methane emission sources using remote sensing, with the aim of reporting the emissions and reducing them in the future.

Methods

Study area

The study is focused on the countries of Indonesia, Malaysia, and Colombia. Indonesia and Malaysia are the world's largest palm oil producers, with 1,231 and 500 POMs listed[6], respectively. Colombia generated more than 1.9 million tons of palm oil in 2023[5] and owns some 76 POMs[6]. We chose these countries for this study due to their high palm oil production and the availability of data from the Carbon Mapper campaign in Colombia.

The UML[6] was used to obtain the facility locations. This list is a compilation of over 2,000 POMs worldwide based on data from processors, traders, and consumer goods manufacturers. Each mill is assigned a "universal PO ID" and the status of its Roundtable on Sustainable Palm Oil (RSPO)[28] certification.

Data from space- and airborne imaging spectrometers

Methane has a weaker absorption window around 1700 nm and a stronger absorption window around 2300 nm, which enables the detection and quantification of methane by sensors sensitive to these wavelengths. Hyperspectral imaging spectrometers, including the GHGSat, EnMAP, PRISMA and EMIT spaceborne instruments and AVIRIS-NG airborne spectrometers, have demonstrated capabilities to identify methane point sources from measurements of solar-reflected radiance in those short-wave infrared bands[22,24,29].

GHGSat is specially designed to detect and quantify methane emissions from point sources. It employs a wide-angle Fabry-Perot imaging spectrometer capable of generating methane enhancement maps using the 1700 nm band with a high spectral resolution of about 0.1 nm and a spatial resolution of 25 meters[26]. On the other hand, EnMAP, PRISMA and EMIT offer a relatively high sensitivity to methane due to multiple spectral channels around 2300 nm and a high spatial sampling (30 m for EnMAP and PRISMA, and 60 m for EMIT), although their data acquisition capacity is limited.

For this study, we obtained several acquisitions from different satellite imaging spectrometers, namely 3 from the GHGSat satellite constellation, and about 30 from EnMAP, 10 from EMIT, and 50 from PRISMA. We also used 2 image acquisitions from the airborne AVIRIS-NG, which is of a similar instrument class than EnMAP, PRISMA and EMIT. A comparative summary of the technical characteristics of these instruments is presented in Table S2. Based on these specifications, AVIRIS-NG is the instrument with the highest sensitivity to methane, while GHGSat has the best performance in terms of detection limit among the satellite instruments. However, PRISMA and EnMAP perform better in terms of spatial coverage.

Detection of methane emissions

Methane concentration enhancement (ΔXCH_4) maps and methane plumes were obtained from a variety of sources, depending on the instrument.

ΔXCH_4 maps from AVIRIS-NG were downloaded from the Carbon Mapper Portal[30]. The analysis methods described in Cusworth et al.[31] were applied to generate the datasets and the plume quantification used in this study. For the official ΔXCH_4 user product from GHGSat, the physically-based methane concentration retrieval described in Jervis et al.[26] was applied. Finally, from EnMAP, PRISMA, and EMIT, we used L1B (spectral radiance) public data to obtain the ΔXCH_4 maps using the matched-filter retrieval algorithm. Our processing of the hyperspectral data is described in Guanter et al. [22].

Once we have obtained the ΔXCH_4 maps, the image is visually inspected to detect potential methane plumes. The overlay of the generated retrievals on a high-resolution image from Google Earth allows us to confirm whether the enhancement comes from a potentially emitting source or may be a retrieval artifact, i.e. pixels that are misled by methane in the concentration enhancement maps[32]. For the detected plume candidates, we check if the direction of the possible emission aligns with the wind speed at 10 m above the surface (U10) derived from the NASA Goddard Earth Observing System-Fast Processing (GEOS-FP) meteorological reanalysis product[33]. Finally, to quantify the emissions, we used the matched filter method. The details of our processing of plume quantification are provided in Roger et al.[29].

As a result, we detected 2 methane plumes with AVIRIS-NG in Colombia, 3 methane plumes with GHGSat in Indonesia, and more than 20 methane enhancements related to POMs from EnMAP, PRISMA and EMIT acquisitions in Indonesia, Malaysia and Colombia.

Bottom-up estimation of methane emission from POMs

In this study, we have obtained the methane emissions related estimates produced by conventional open pond systems of monitored mills. We selected baseline values from a typical POME pond treatment system (Table S3). We obtained CPO production data for each mill through information provided by the RSPO and the Nusantara Atlas portal[34]. Using these average values and the equations explained in the S.I. Methodology, we estimated methane emissions in kilograms per year from the mills, as well as their carbon dioxide equivalent (CO_{2eq}).

Results and Discussion

Plume detections in Colombia with AVIRIS-NG

During the 2023 Carbon Mapper campaign, 2 methane plumes were detected over the ponds of POM in César province, Colombia, using the AVIRIS-NG airborne spectrometer. Fig. 2 shows the methane emissions detected in two overpasses within 13-minute intervals on March 19, 2023. The estimated quantities for these plumes are 130 ± 80 kg/h and 142 ± 51 kg/h, respectively, which is in the range of emissions reported by on-site studies. The wind speed has been estimated at 0.9m/s with southeast direction. The raw ΔXCH_4 maps are presented in Fig. S1.

Established in 2008, this mill has a production capacity of 45 t FFB/h by 2023, producing both CPO and CKO. It currently operates on a planted area of 5,500 hectares and the total volume of FFB in 2023 was approximately 102,749 tons, while its production of CPO was roughly 35,711 t/y[28]. Considering the estimated methane emissions discussed in the Methodology, this mill could have emitted 1,279,082 kg CH_4 directly into the atmosphere by 2023, which corresponds to annual GHG emissions of roughly 107,442 t CO_{2eq} (Table S4).
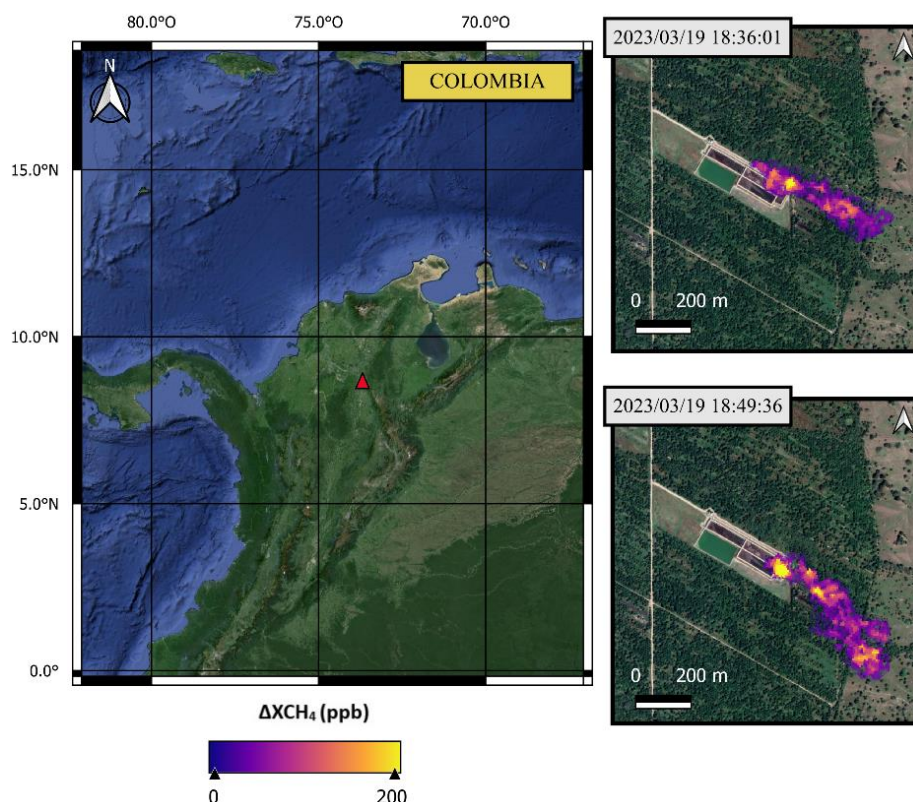
Figure 2. Methane plumes detected with AVIRIS-NG over a POM in César province, Colombia (latitude: 8.614°, longitude: -73.680°). The left panel shows a Google Earth base map with the location of the monitored POM. Panels at the right show a Google Earth base map with the two methane plumes from AVIRIS-NG overpasses on March 19, 2023, within a 13-minutes difference.

Plume detections in Indonesia with GHGSat

Additionally, we detected 3 methane emissions in Indonesia with GHGSat satellites. Two of the plumes are enhancements found on top of the ponds, without tails extending beyond the facility as in the case of AVIRIS-NG (Fig. 3A and B). These may be due to the relatively low emission. On the other hand, we do find a complete plume in the July 8 acquisition (Fig. 3C). The estimated methane emission is roughly 515 ± 303 kg/h. The wind speed has been estimated at 2.1m/s with northwest direction.

The detection of these emissions coincides with the high season of palm oil production in Indonesia, which is in the summer-autumn. Mill A is located in the North Sumatra area of Indonesia and has a processing capacity of 30 t FFB/h. Mill B and mill C, located in the Riau area, have a processing capacity of 40 t FFB/h and 20 t FFB/h, respectively. None of these three facilities are RSPO certified, so we used the 2020 data provided by Nusantara Atlas[34] to estimate their total methane emissions. According to these records, the estimated methane emissions by these mills in 2020 are: mill A emitted ~534,649 kg CH_4, mill B emitted ~838,490 kg CH_4, and mill C emitted ~393,993 kg CH_4. These estimated methane emissions from the mills correspond to more than

148,439 t CO_{2eq} emitted directly into the atmosphere in 2020 (Table S4). More specifically, it is estimated that Indonesia has less than 10% of its mills with biogas systems[16], so considering their CPO production in 2023 of about 47 million tons, methane emissions could reach more than 1,151,000 t/y. This is equivalent to the GHG emissions produced by more than 27,478,423 gasoline vehicles driving more than 17,000 km yearly[35].
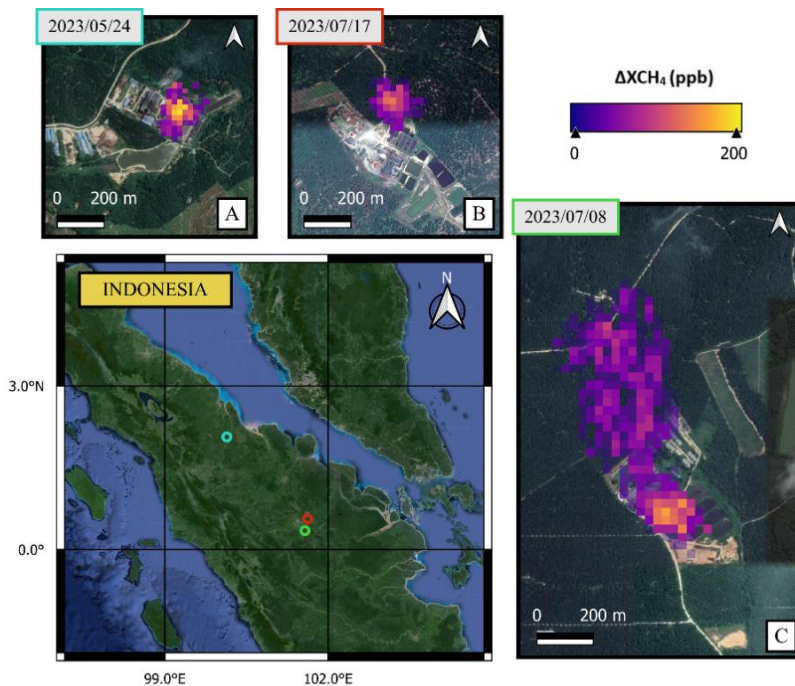
Figure 3. Methane plumes detected with GHGSat in Indonesia. The bottom-left panel shows a Google Earth base map with the locations of the monitored POMs in Indonesia. The bottom-right panel shows a methane plume over the ponds from a mill on June 8, 2023 (C; latitude: 0.423°, longitude: 101.589°). The upper-left panel show the methane retrievals enhancement in different mills, on May 24 (A; latitude: 0.536°, longitude: 101.602°) and July 17, 2023 (B; latitude: 2.063°, longitude: 100.147°). Backgrounds from Google Earth.

Test of plume detections with PRISMA, EnMAP and EMIT

We have explored the capability of the PRISMA, EnMAP, and EMIT satellites, which are less sensitive to methane plumes than AVIRIS-NG and GHGSat, to detect methane plumes from POMs in Indonesia, Malaysia, and Colombia. Detecting emissions from these sources using these satellites poses several challenges. In-situ studies determine that methane emissions from these mills may typically be in the 100-450 kg/h/pond range, which is below the ~500 kg/h detection limit typically assumed for these systems[24,29]. Additionally, since in this case the methane-emitting source is a dark, liquid surface, and the area around the mills is heterogeneous and vegetated, there is a greater likelihood of retrieval artifacts, further complicating plume detection from these satellites.

Despite these challenges, our study identified over 20 potential methane enhancements over ponds within POMs in Colombia, Indonesia and Malaysia using these satellites, some of which

are shown in Fig. S2. It should be noted that almost all of these emissions come from mills in Indonesia. This could be attributed to more than 30% of Malaysia's mills having already implemented biogas systems[3], and several projects were currently ongoing to increase the number of mills with this system, so their methane emissions have been reduced.

Several of those detections correspond to ponds with apparently similar spectral characteristics as those of other ponds from which no enhancement was found (see Fig. S3). This suggests that the type of surface and pond composition (water and organic matter) alone cannot explain the methane concentration enhancements that we detect. More specifically, we detected methane enhancements over the same pond as AVIRIS-NG in Colombia and GHGSat in Indonesia with an EnMAP acquisition on January 27, 2024, and a PRISMA acquisition on September 16, 2023, respectively (see Figs. 4 and S2, respectively).

To better understand these enhancements, we have carried out some additional tests with the EnMAP scene. We carefully checked whether the boundaries of the methane enhancement observed in the retrieval matches the shape of the pond observed in the radiance image, which would indicate that it is a retrieval artifact caused by the pond spectral reflectance. Additionally, we compared the pixels of the Normalized Difference Water Index (NDWI) using the 1600 nm band of the SWIR, where water absorption is dominated[36], to account for potential artifacts introduced by moist land or adjacent vegetation, as these could also affect the SWIR surface albedo and contribute to the observed enhancements. As shown in Fig. 4, we do not observe a direct correlation between the possible methane enhancement retrieval pixels and the radiance and NDWI pixels. This again suggests that the observed enhancements cannot be solely due to the surface of these ponds.
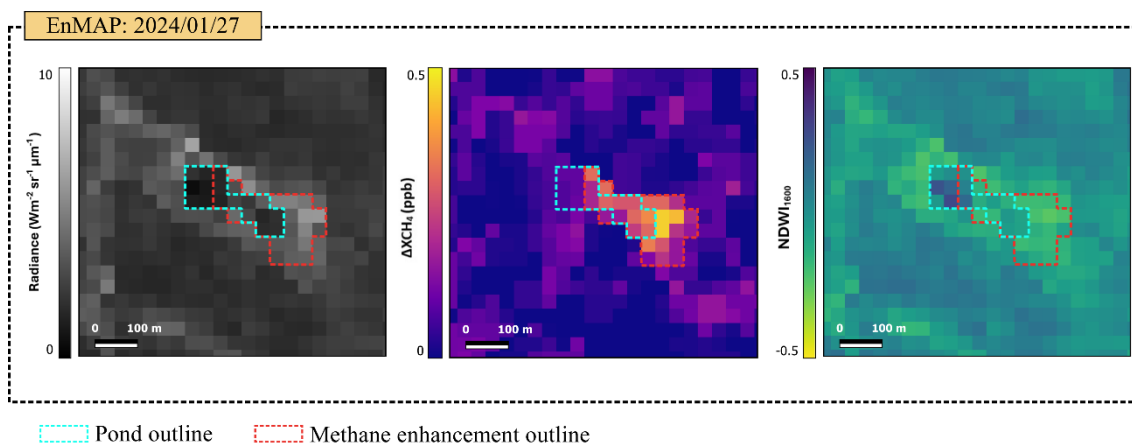
Figure 4. Comparison between the pond and potential methane enhancement contours in the radiance band, ΔXCH_4 map, and $NDWI_{1600}$. EnMAP image of 2024/01/27.

We also compared the EnMAP image indicating possible methane enhancement with another image taken four days later (January 31), which showed no methane enhancement (see Fig. S4). We can observe that, although both have similar radiance levels, we can see a possible methane enhancement on the January 27 dataset, whereas the image from January 31 does not show any

enhancement. The difference could be due to a non-visible change in the radiance image, such as adding or removing effluent or maybe a real methane enhancement. Additionally, the unit spectrum of methane absorption in the 2300 nm window, where the matched filter recovery is applied, is shown along with the image radiance and pond pixels (see Fig. S5). The lack of a clear correlation between these spectra and the absorption features makes it difficult to link the presence of methane to the pond pixel enhancement values.

On the other hand, the downscaling of AVIRIS-NG data to EnMAP's spatial resolution and noise (see Fig. S6) suggests that emissions of about 100 kg/h, as detected by AVIRIS-NG in Colombia, would not be detected by EnMAP on this heterogeneous palm oil surface. For this reason, the possible methane enhancement detected by this sensor should be higher than this quantity. To investigate further, we analyzed both EnMAP images to determine the emission rates that would be detectable (see Fig. S7). The results indicate an underestimation of methane enhancement due to the spectrum related to the pond surface, which exhibits a non-negligible deviation from the scene mean value. Both days show a similar response to methane, which suggests that the January 27 enhancement might happen due to methane emission. In contrast, as shown in Fig. 4, vegetation pixels near the pond exhibit a more favorable background for an unbiased methane enhancement. Extrapolating these results, it is estimated that this possible methane emission would be 700 kg/h, which matches our quantification of 785.1 ± 262.5 kg/h.

Consequently, one possible scenario is that the methane emissions reported in previous in-situ studies could be higher than we estimate because if so, satellite instruments with technical specifications such as EnMAP, PRISMA, or EMIT would be able to detect them.

Discussion and conclusions

The increased atmospheric methane concentrations in recent decades are a primary environmental concern due to their growing impact on climate change. Many of these emissions are anthropogenic, including those from the agricultural and waste sectors, such as POM. The conventional method of treating the POME using the open ponding system is not environmentally sustainable. Transitioning to sustainable management practices utilizing biomass residues and biogas not only addresses the environmental concerns associated with POME but also aligns with global efforts towards sustainable development goals. Implementing biogas systems directly benefits for palm oil exporting countries: the generation of energy that contributes to the country's economic potential, the reduction of its carbon footprint and the mitigation of GHG emissions.

The methane plumes presented in this paper demonstrate that detection of these emissions from POMs is possible with the AVIRIS-NG airborne instrument and GHGSat satellite constellation, and that our flux rate estimates are consistent with previous literature measurements. This results in an accurate understanding of emission sources and their

behaviour and supports using these technologies for monitoring methane emissions. However, the limited amount of confirmed plume detections makes it difficult to extract conclusions on the typical emission factors for these sources. For this reason, it could be useful to carry out flight campaigns to characterize the POMs and examine the distribution of the flux rates of the emitting ponds, which can help improve emissions mitigation and monitoring strategies. In addition, this could contribute to developing a global map of water-saturated soils and inundated areas emitting methane to improve the methane balance[37].

This study is unable to confirm that EnMAP, PRISMA and EMIT enhancements are real emissions due to the worse spatial and spectral resolution of these hyperspectral satellites (compared to AVIRIS-NG and GHGSat) and the lack of ground-based data or another reliable measurement source for our specific cases to verify our observations.

Consequently, we consider that further research is necessary, as the results of the performed test are insufficient to confidently determine whether the observed enhancements are retrieval artifacts due to the emission source properties or genuine methane emissions. If the latter, it would possibly indicate that the emissions may be higher than previously reported in the literature. It should be noted that these estimates of methane emissions from palm oil production depend on many factors, such as the growing season of the palm, which varies the monthly CPO production. Oil palm is a perennial crop with 25-30 years of productive life, starting FFB production in its third year, so many of the current hectares need to be replanted, which may affect the palm oil production of each of these mills. Therefore, the detected enhancements could correspond to a high production period of these mills. Additionally, the amount of methane emitted by each pond depends on the phase of methanogenesis and the effluent retention time specific to each POM, explaining why enhancements are not always detected.

In the future, studies could benefit from using thermal bands with high spatial resolution to distinguish between different types of ponds (cooling, anaerobic, facultative). Correlating the temperature of anaerobic ponds with methane enhancements could provide an additional method to validate methane detections from space. Additionally, a recent study by Fahlen *et al.*[38] highlights the importance of accounting for surface variability in data-driven methane retrievals, such as the matched-filter used in this study, especially over surface types with an abnormal spectral response. This concept is particularly relevant for POMs and should be considered in future studies with these sources.

This study opened up a previously unexplored area of methane emissions from space with an immediate and cost-effective mitigation potential, highlighting the importance of investing in advanced technologies to address environmental challenges effectively. The next generation of satellites needs to focus on lower but consistent methane emissions from areas sources such as agriculture, wetlands, and permafrost.

Bibliography

1. Etminan, M., Myhre, G., Highwood, E. J., & Shine, K. P. (2016). Radiative forcing of carbon dioxide, methane, and nitrous oxide: A significant revision of the methane radiative forcing. Geophysical Research Letters, 43(24). https://doi.org/10.1002/2016GL071930

2. Yusuf, R. O., Noor, Z. Z., Abba, A. H., Hassan, M. A. A., & Din, M. F. M. (2012). Methane emission by sectors: A comprehensive review of emission sources and mitigation methods. Renewable and Sustainable Energy Reviews, 16(7), 5059-5070. https://doi.org/10.1016/j.rser.2012.04.008

3. Nasrin, A. B., Abdul Raman, A. A., Bukhari, N. A., Sukiran, M. A., Buthiyappan, A., Subramaniam, V., Aziz, A. A., & Loh, S. K. (2022). A critical analysis on biogas production and utilisation potential from palm oil mill effluent. Journal of Cleaner Production, 361, 132040. https://doi.org/10.1016/j.jclepro.2022.132040

4. Danylo, O., Pirker, J., Lemoine, G., Ceccherini, G., See, L., McCallum, I., Hadi, Kraxner, F., Achard, F., & Fritz, S. (2021). A map of the extent and year of detection of oil palm plantations in Indonesia, Malaysia and Thailand. Scientific Data, 8(1), 96. https://doi.org/10.1038/s41597-021-00867-1

5. United States Department of Agriculture. (2023). *Oilseeds: World markets and trade*. Retrieved from https://fas.usda.gov/data/production/commodity/4243000

6. Rainforest Alliance (2023). The Universal Mill List. Retrieved June 6, 2024, from https://www.rainforest-alliance.org/business/certification/the-universal-mill-list/

7. Viridis Engineering. (2024). Air pollution & dust emissions control. Retrieved May 29, 2024, from https://www.viridis-engineering.com/solutions/air-pollution-dust-emissions-control/

8. Yacob, S., Hassan, M. A., Shirai, Y., Wakisaka, M., & Subash, S. (2005). Baseline study of methane emission from open digesting tanks of palm oil mill effluent treatment. Chemosphere, 59(11), 1575-1581. https://doi.org/10.1016/j.chemosphere.2004.11.040

9. Akhbari, A., Kutty, P. K., Chuen, O. C., & Ibrahim, S. (2019). A study of palm oil mill processing and environmental assessment of palm oil mill effluent treatment. Environmental Engineering Research, 25(2), 212-221. https://doi.org/10.4491/eer.2018.452

10. Lee, Z. S., Chin, S. Y., Lim, J. W., Witoon, T., & Cheng, C. K. (2019). Treatment technologies of palm oil mill effluent (POME) and olive mill wastewater (OMW): A brief review. Environmental Technology & Innovation, 15, 100377. https://doi.org/10.1016/j.eti.2019.100377

11. Poh, P. E., & Chong, M. F. (2009). Development of anaerobic digestion methods for palm oil mill effluent (POME) treatment. Bioresource Technology, 100(1), 1-9. https://doi.org/10.1016/j.biortech.2008.06.022

12. Chung, A. Y. K., Qamaruz Zaman, N., Yaacof, N., Yusoff, S., Abd. Manaf, F. Y., Mohamed Halim, R., & Abd. Majid, R. (2019). The Effectiveness of Gas Recovery Systems for Managing Odour from Conventional Effluent Treatment Ponds in Palm Oil Mills in Malaysia. Civil and Environmental Engineering Reports, 29(3), 70-85. https://doi.org/10.2478/ceer-2019-0025

13. Jamaludin, N. F., Ab Muis, Z., Hashim, H., Mohamed, O. Y., & Lek Keng, L. (2024). A holistic mitigation model for net zero emissions in the palm oil industry. Heliyon, 10(6), e27265. https://doi.org/10.1016/j.heliyon.2024.e27265

14. Ohimain, E. I., & Izah, S. C. (2017). A review of biogas production from palm oil mill effluents using different configurations of bioreactors. Renewable and Sustainable Energy Reviews, 70, 242-253. https://doi.org/10.1016/j.rser.2016.11.221

15. Lam, M. K., & Lee, K. T. (2011). Renewable and sustainable bioenergies production from palm oil mill effluent (POME): Win–win strategies toward better environmental protection. Biotechnology Advances, 29(1), 124-141. https://doi.org/10.1016/j.biotechadv.2010.10.001

16. Rajani, A., Kusnadi, Santosa, A., Saepudin, A., Gobikrishnan, S., & Andriani, D. (2019). Review on biogas from palm oil mill effluent (POME): Challenges and opportunities in Indonesia. IOP Conference Series: Earth and Environmental Science, 293(1), 012004. https://doi.org/10.1088/1755-1315/293/1/012004

17. El Palmicultor (2023). *Biogás, un impulso hacia la economía circular y la descarbonización del sector palmero colombiano*. Retrieved from https://elpalmicultor.com/biogas-impulso-economia-descarbonizacion-sector/

18. Enström, A., Haatainen, T., Suharto, A., Giebels, M., & Lee, K. Y. (2019). Introducing a new GHG emission calculation approach for alternative methane reduction measures in the wastewater treatment of a palm oil mill. Environment, Development and Sustainability, 21(6), 3065-3076. https://doi.org/10.1007/s10668-018-0181-4

19. Yacob, S., Ali Hassan, M., Shirai, Y., Wakisaka, M., & Subash, S. (2006). Baseline study of methane emission from anaerobic ponds of palm oil mill effluent treatment. Science of The Total Environment, 366(1), 187-196. https://doi.org/10.1016/j.scitotenv.2005.07.003

20. Schuchardt, F., Wulfert, K., Darnoko, D., & Herawan, T. (2008). Effect of new palm oil mill processes on the EFB and POME utilization. Journal of Oil Palm Research, 20, 115-126.

21. Conil, P., & Kervyn, B. (2009). Biogas from palm oil mill effluent: from the first biodigesters in the 80'to. In Palm Oil: Proceedings of chemistry, processing technology & bio energy conference (Vol. 1, p. 159). Malaysian Palm Oil Board, Ministry of Plantation Industries and Commodities, Malaysia.

22. Guanter, L., Irakulis-Loitxate, I., Gorroño, J., Sánchez-García, E., Cusworth, D. H., Varon, D. J., Cogliati, S., & Colombo, R. (2021). Mapping methane point emissions with the PRISMA spaceborne imaging spectrometer. Remote Sensing of Environment, 265, 112671. https://doi.org/10.1016/j.rse.2021.112671

23. Irakulis-Loitxate, I., Guanter, L., Liu, Y.-N., Varon, D. J., Maasakkers, J. D., Zhang, Y., Chulakadabba, A., Wofsy, S. C., Thorpe, A. K., Duren, R. M., Frankenberg, C., Lyon, D. R., Hmiel, B., Cusworth, D. H., Zhang, Y., Segl, K., Gorroño, J., Sánchez-García, E., Sulprizio, M. P., … Jacob, D. J. (2021). Satellite-based survey of extreme methane emissions in the Permian basin. Science Advances, 7(27), eabf4507. https://doi.org/10.1126/sciadv.abf4507

24. Cusworth, D. H., Jacob, D. J., Varon, D. J., Chan Miller, C., Liu, X., Chance, K., Thorpe, A. K., Duren, R. M., Miller, C. E., Thompson, D. R., Frankenberg, C., Guanter, L., & Randles, C. A. (2019). Potential of next-generation imaging spectrometers to detect and quantify methane point sources from space. Atmospheric Measurement Techniques, 12(10), 5655-5668. https://doi.org/10.5194/amt-12-5655-2019

25. Thorpe, A. K., Green, R. O., Thompson, D. R., Brodrick, P. G., Chapman, J. W., Elder, C. D., Irakulis-Loitxate, I., Cusworth, D. H., Ayasse, A. K., Duren, R. M., Frankenberg, C., Guanter, L., Worden, J. R., Dennison, P. E., Roberts, D. A., Chadwick, K. D., Eastwood, M. L., Fahlen, J. E., & Miller, C. E. (2023). Attribution of individual methane and carbon dioxide emission sources using EMIT observations from space. Science Advances, 9(46), eadh2391. https://doi.org/10.1126/sciadv.adh2391

26. Jervis, D., McKeever, J., Durak, B. O. A., Sloan, J. J., Gains, D., Varon, D. J., Ramier, A., Strupler, M., & Tarrant, E. (2021). The GHGSat-D imaging spectrometer. Atmospheric Measurement Techniques, 14(3), 2127-2140. https://doi.org/10.5194/amt-14-2127-2021

27. Thorpe, A. K., O'Handley, C., Emmitt, G. D., DeCola, P. L., Hopkins, F. M., Yadav, V., Guha, A., Newman, S., Herner, J. D., Falk, M., & Duren, R. M. (2021). Improved methane emission estimates using AVIRIS-NG and an Airborne Doppler Wind Lidar. Remote Sensing of Environment, 266, 112681. https://doi.org/10.1016/j.rse.2021.112681

28. Roundtable on Sustainable Palm Oil (RSPO). (2024). Members: 2-0501-14-000-00. Retrieved September 10, 2024, from https://rspo.org/es/members/2-0501-14-000-00/

29. Roger, J., Irakulis-Loitxate, I., Valverde, A., Gorroño, J., Chabrillat, S., Brell, M., & Guanter, L. (2024). High-Resolution Methane Mapping With the EnMAP Satellite Imaging Spectroscopy Mission. IEEE Transactions on Geoscience and Remote Sensing, 62, 1-12. https://doi.org/10.1109/TGRS.2024.3352403

30. Carbon Mapper data (2023). Retrieved from https://data.carbonmapper.org [19/03/2023]

31. Cusworth, D. H., Thorpe, A. K., Ayasse, A. K., Stepp, D., Heckler, J., Asner, G. P., Miller, C. E., Yadav, V., Chapman, J. W., Eastwood, M. L., Green, R. O., Hmiel, B., Lyon, D. R., & Duren, R. M. (2022). Strong methane point sources contribute a disproportionate fraction of total emissions across multiple basins in the United States. Proceedings of the National Academy of Sciences, 119(38), e2202338119. https://doi.org/10.1073/pnas.2202338119

32. Roger, J., Guanter, L., Gorroño, J., & Irakulis-Loitxate, I. (2024). Exploiting the entire near-infrared spectral range to improve the detection of methane plumes with high-resolution imaging spectrometers. Atmospheric Measurement Techniques, 17(4), 1333-1346. https://doi.org/10.5194/amt-17-1333-2024

33. Molod, A., Takacs, L., Suarez, M., Bacmeister, J., Song, I.-S., & Eichmann, A. (2012). The GEOS-5 Atmospheric General Circulation Model: Mean Climate and Development from MERRA to Fortuna. Retrieved from https://portal.nccs.nasa.gov/datashare/gmao/geos-fp/das/

34. Nusantara Atlas (2024). Nusantara Atlas. Retrieved May 29, 2024, from https://map.nusantara-atlas.org/

35. U.S. EPA (Environmental Protection Agency, 2024). Greenhouse Gas Equivalencies Calculator. Retrieved from https://www.epa.gov/energy/greenhouse-gas-equivalencies-calculator

36. Chen, D., Huang, J., & Jackson, T. J. (2005). Vegetation water content estimation for corn and soybeans using spectral indices derived from MODIS near- and short-wave infrared bands. Remote Sensing of Environment, 98(2-3), 225-236. https://doi.org/10.1016/j.rse.2005.07.008

37. Saunois, M., Martinez, A., Poulter, B., Zhang, Z., Raymond, P., Regnier, P., Canadell, J. G., Jackson, R. B., Patra, P. K., Bousquet, P., Ciais, P., Dlugokencky, E. J., Lan, X., Allen, G. H., Bastviken, D., Beerling, D. J., Belikov, D. A., Blake, D. R., Castaldi, S., … Zhuang, Q. (2024). Global Methane Budget 2000–2020. https://doi.org/10.5194/essd-2024-115

38. Fahlen, J. E., Brodrick, P. G., Coleman, R. W., Elder, C. D., Thompson, D. R., Thorpe, A. K., Green, R. O., Green, J. J., Lopez, A. M., & Xiang, C. (2024). Sensitivity and Uncertainty in Matched-Filter-Based Gas Detection With Imaging Spectroscopy. IEEE Transactions on Geoscience and Remote Sensing, 62, 1-10. https://doi.org/10.1109/TGRS.2024.3440174

Acknowledgments

Author contributions

Conceptualization: All authors. Methodology: A.V., J.R. and L.G. Formal Analysis: All authors Investigation: A.V. and J.G. Supervision: L.G. Writing-original draft: A.V. Writing-review and editing: All authors.

Competing interests

The authors declare no competing interests.

Detecting methane emissions from palm oil mills using imaging spectrometers

SUPPORTING INFORMATION

Adriana Valverde[1*], Javier Roger[1], Javier Gorroño[1], Itziar Irakulis-Loitxate[2,1] and Luis Guanter[1,3]

[1] Research Institute of Water and Environmental Engineering (IIAMA), Universitat Politècnica de València, Spain.

[2] International Methane Emission Observatory (IMEO), United Nations Environment Programme, Paris, France.

[3] Environmental Defense Fund, Amsterdam, Netherlands.

* Corresponding author's email: avaligl@doctor.upv.es

Summary:

Number of pages: 7

Tables: S1 to S3

Figures: S1 to S7

Introduction

Table of specific properties of palm oil mill effluent with the typical range of values for each parameter. These properties make the POME require pretreatment before discharge into the environment.

Parameters	Range
Temperature (°C)	80-90
pH	4 - 5
Chemical Oxygen Demand (COD) (mg/L)	15,000-100,000
Biochemical Oxygen Demand (BOD) (mg/L)	10,250 – 43,750
Total Solid (TS) (mg/L)	11,500 – 79.000
Total Suspended Solid (TSS) (mg/L)	5,000- 45,000
Oil and Grease (mg/L)	130 -18,000

Table S1. POME characteristics.

Methodology

Data from space- and airborne imaging spectrometer

	AVIRIS-NG	GHGSat	EMIT	EnMAP	PRISMA
Píxel size (m^2)	3x3	25x25	60x60	30x30	30x30
Spectral range (nm)	2200-2510	1600–1700	2200–2510	2100–2450	2100–2450
Spectral resolution (nm)	5	0.3–0.7	7.4	10	10
Signal-to-noise ratio (SNR)	200 - 400	n/a	200-300	>180	180

Table S2. A comparative table of imaging spectrometer sensors used in this study. The table is focused on the bands used for methane retrieval.

Bottom-up estimation of methane emission from POMs

Variable	Value
Degradable organic component (DOC)	53 kg DOC/m^3 POME
POME produced	3 m^3 POME/t CPO
Biogas	28 m^3 biogas/ m^3 POME
Density of methane	0.656 kg/ m^3
Fraction of methane in biogas	65%
Maximum methane producing capacity	0.25 kg CH_4/Kg COD
Global warming potential (GWP_{CH4})	84

Table S3. Baseline values for typical POME ponding treatment system.

As expressed in the formula [1], we calculated the annual production of POME using the annual production of CPO [tons] and the predetermined average POME production per ton of CPO, which is estimated at 3 m3, according to previous studies.

$$POMEouput = CPOproduced \: x \: 3$$

where $POME_{ouput}$ represents the POME produced per year [m^3]; $CPO_{produced}$ represents the amount of crude palm oil produced by the mill in a year [tons], and 3 represents the average value of m^3/POME per t/CPO.

In the estimation of the amount of biogas generated by the water waste, we assume that for each m^3 of POME generated, biogas production is estimated at 28 m^3, as shown in Eq. (2)

$$BIOGAStotal = POMEouput \: x \: 28$$

where $BIOGAS_{total}$ represent the volume of biogas produced from POME [m^3]; $POME_{ouput}$ represents the volume of POME per year [m^3] and 28 is the amount of biogas produced per tons POME [m^3].

In this study, we considered that the proportion of methane in the biogas generated in open pond systems typically ranges from 55-70%, according by previous research (Yacob et al., 2005; Loh et al., 2017). Therefore, we used an average value of 0.65 for our calculations. The amount of methane in kilograms was determined by multiplying this proportion by the density of methane (0.656 kg/ m^3) for specific POME temperature conditions.

$$METHANEtotal = BIOGAStotal \: x \: 0.65 \: x \: 0.656$$

where $METHANE_{total}$ represents the total of methane emitted per year (kg); $BIOGAS_{total}$ represent the volume of biogas produced from POME [m^3]; 0.65 represents the average concentration of methane in the biogas; and 0.656 represents the density of methane [kg/ m^3].

Finally, according to the GWP values for 20-year time horizon from IPCC Fifth Assessment Report (AR5), we used the value 84 for GWP_{CH4} to calculate the carbon dioxide equivalent (CO_{2eq}) of the methane emissions from palm oil mills.

Results

Plume detections in Colombia with AVIRIS-NG
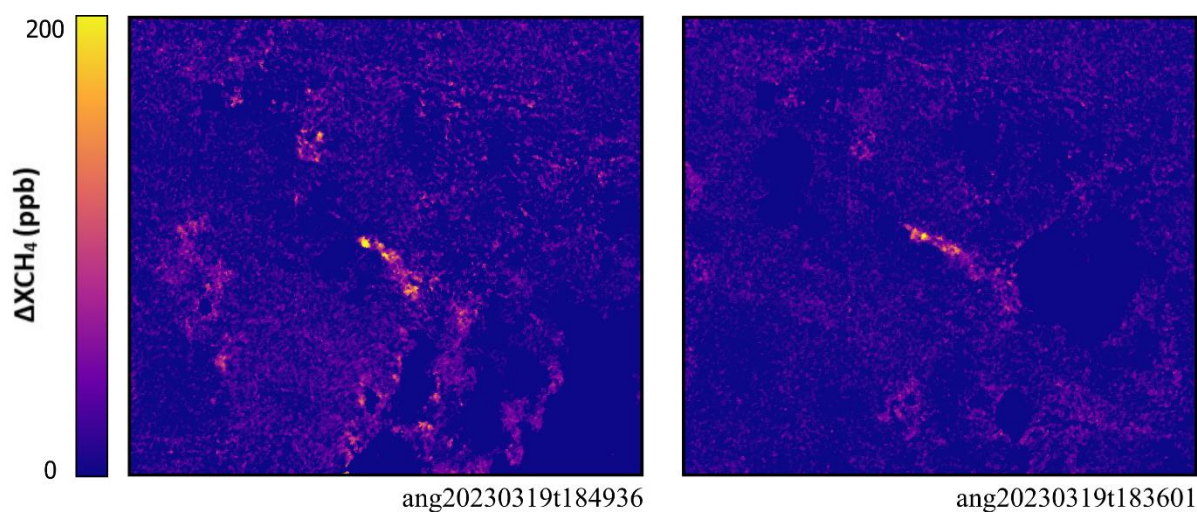
Figure S1. AVIRIS-NG methane enhancements maps with their image identifier.

Location (lat/lon)	Production (t/y)	POME (m^3/y)	Biogas (m^3/y)	CH$_4$ (t/y)	CO$_{2eq}$ (t/y)
8.614, -73.680	35,711.00	107,133.00	2,999,724.00	1,279.08	107,442.91
0.536, 101.602	23,410.00	70,230.00	1,966,440.00	838.49	70,433.16
0.423, 101.58	11,000.00	33,000.00	924,000.00	393.99	33,095.46
2.063, 100.146	14,927.00	44,781.00	1,253,868.00	534.65	44,910.54

Table S4. The table shows the coordinates of the mills, estimated CPO production for a year (2022 for Colombia's mill, 2020 for Indonesia's mills), estimated POME production, estimated biogas production, estimated methane emitted, and estimated CO$_{2eq}$.

Test of plume detections with PRISMA, EnMAP and EMIT
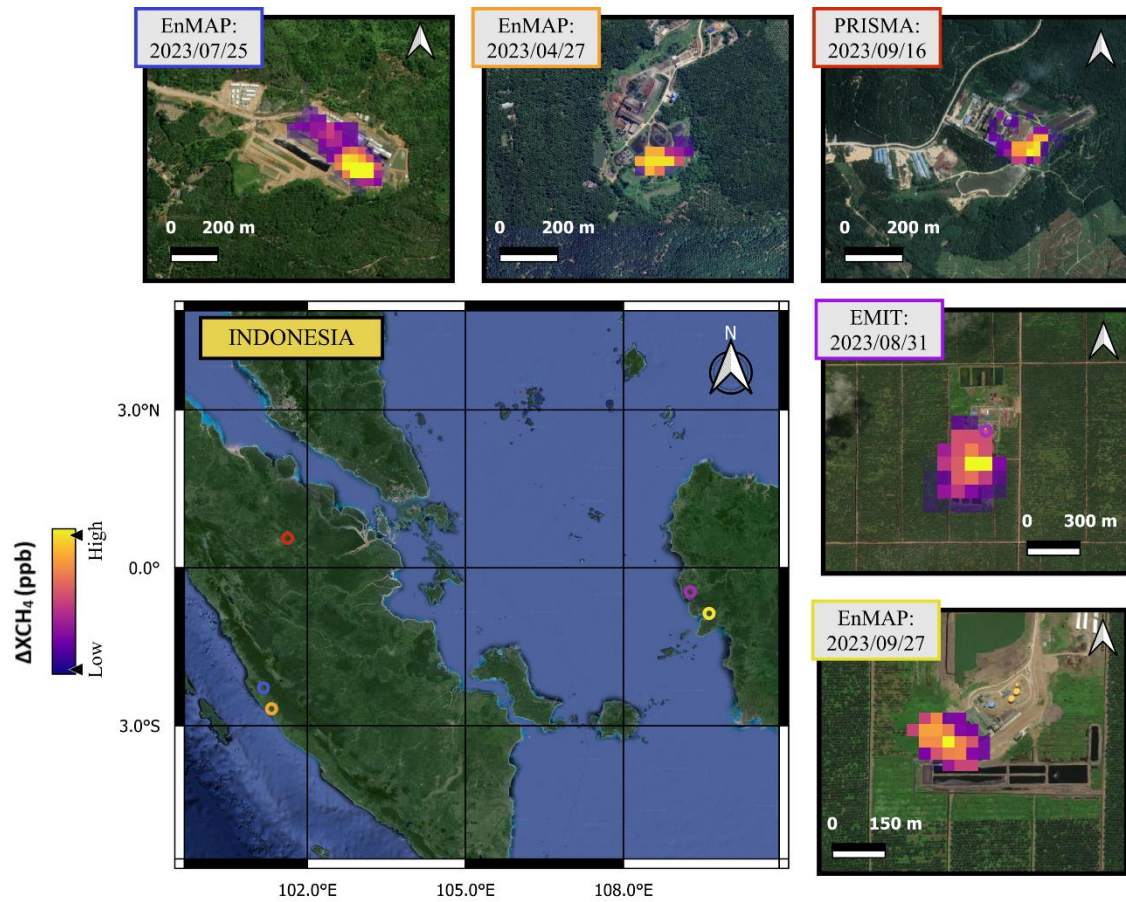
Figure S2. Potential methane enhancements with EnMAP, PRISMA and EMIT satellites at different palm oil mills in Indonesia. The central panel shows a Google Earth base map with the locations of the monitored palm oil mills. The other panels show the potential methane enhancements from: EnMAP image of July 25, 2023 (lat: -2.27°, lon: 101.16°); EnMAP image of April 27, 2023 (lat: -2.67°, lon: 101.32°); PRISMA image of September 16, 2023 (lat: 0.53°, lon: 101.60°); EMIT image of August 31, 2023 (lat: -0.45°, lon: 109.26°); and EnMAP image of September 27, 2023 (lat: -0.86°, lon: 109.62°). Backgrounds from Google Earth.
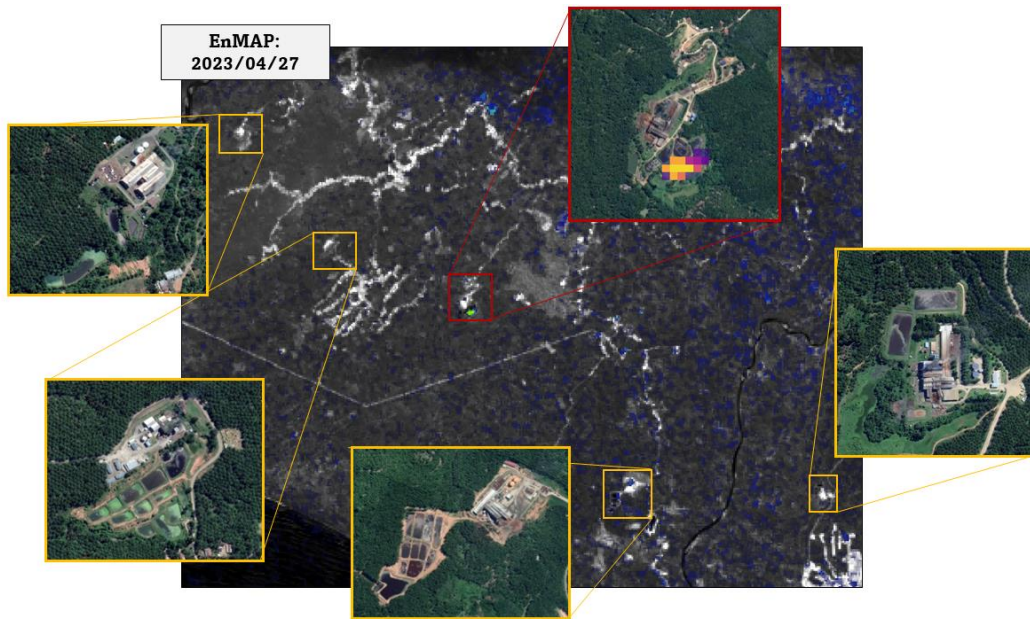
Figure S3. EnMAP retrieval image above its radiance image. The centre panel shows an EnMAP retrieval from 27 April 2023 above its radiance image, with potential methane enhancements in a palm oil mill pond (lat: -2.67°, lon: 101.32°). The other high-resolution images from Google Earth correspond to palm oil mills in this area, which don't have methane enhancements.
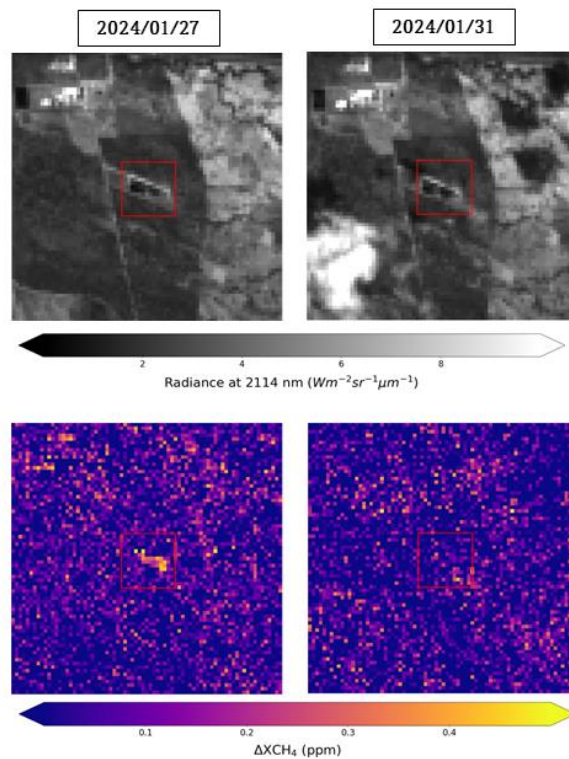
Figure S4. Comparison between two EnMAP images on different days of the same POM in Colombia. Top row: radiance band comparison at 2114 nm from January 27 and 31, 2024. Bottom row, comparison of the retrieval maps from January 27 and 31, 2024.
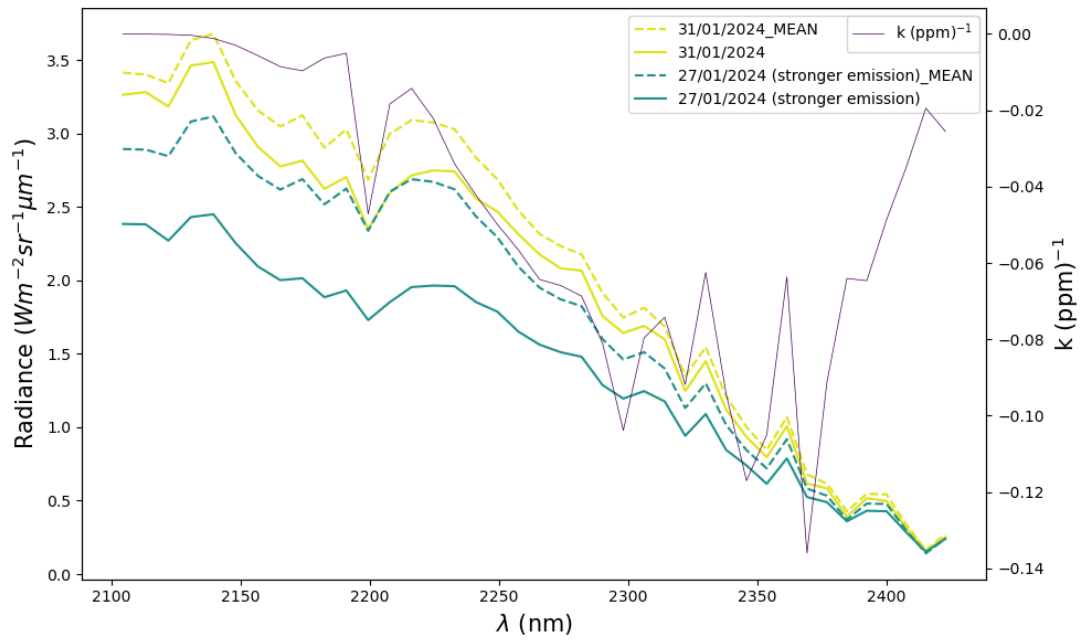
Figure S5. Comparison between spectres of EnMAP images from different days. The average radiance spectra (dashed lines) from the EnMAP images acquired on 31/01/2024 (in yellow) and on 27/01/2024 (in green) are shown along with the spectra associated with the pond pixels (solid lines). In addition, the unit methane absorption spectrum (in purple) is shown to illustrate whether the differences between the mean and pond spectra are related to methane absorption.
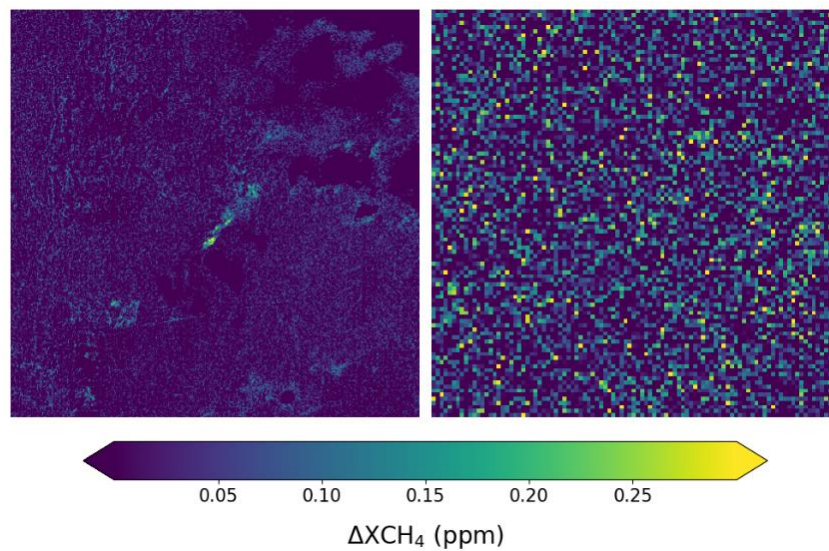
Figure S6. Replication of EnMAP data from AVIRIS-NG. We applied a nearest neighbours down sampling to an AVIRIS-NG methane retrieval (left) to match the EnMAP spatial resolution. Based on retrievals obtained from EnMAP data capturing the same area as the AVIRIS-NG scene, we added random noise to the resampled retrieval to obtain an EnMAP-like retrieval (right).

We use WRF-LES simulated plumes associated with similar U10 values to those of the EnMAP acquisitions on the 27th and 31st of January (1.88 m/s and 2.26 m/s, respectively). Then, we collapse these plumes into 2-dimensional methane enhancement maps at EnMAP's spatial resolution. The default emission rate value for the emission is 100 kg/h, but we simply scale the methane maps to acquire plumes with an equivalent Q of 200 kg/h, 300 kg/h, 400 kg/h, and 500 kg/h, which covers the range of methane emission rates from palm oil mills according to the literature. Now, we associate the maximum enhancement value of the methane maps with the plume Q values. For instance, we get the mean of the maximum enhancement values for the plumes with U10 values similar to those of 27th January and with Q = 100 kg/h. We repeat this process for the other Q values and the plumes related to the wind speed similar to that on the 31st. Then, we can relate the enhancement to flux rate values from realistic emissions, which will help us to better understand the enhancement values over the pond in the EnMAP acquisition from Figure 4. Next, we artificially integrate the resulting enhancement values over the same pond as in Guanter *et al.* (2021) for both acquisitions. We then apply the matched filter method and compare the retrieved values to the ones that were added. This comparison, as shown in Figure S7, reveals a non-negligible underestimation of the retrieved values. If we repeat this exercise in close-to-the-pond pixels that cover a vegetation area, we observe that the retrieved values are unbiased. This comparison underscores the accuracy of our method. Most of the scene area is made up of vegetation, so methane enhancement over this kind of soil will result in a matched filter with better performance. On the other hand, enhancements over the pond will not be accurately retrieved due to an important deviation from the mean spectra. Nevertheless, the response to methane is similar to both ponds and it could be observed under relatively strong emissions.
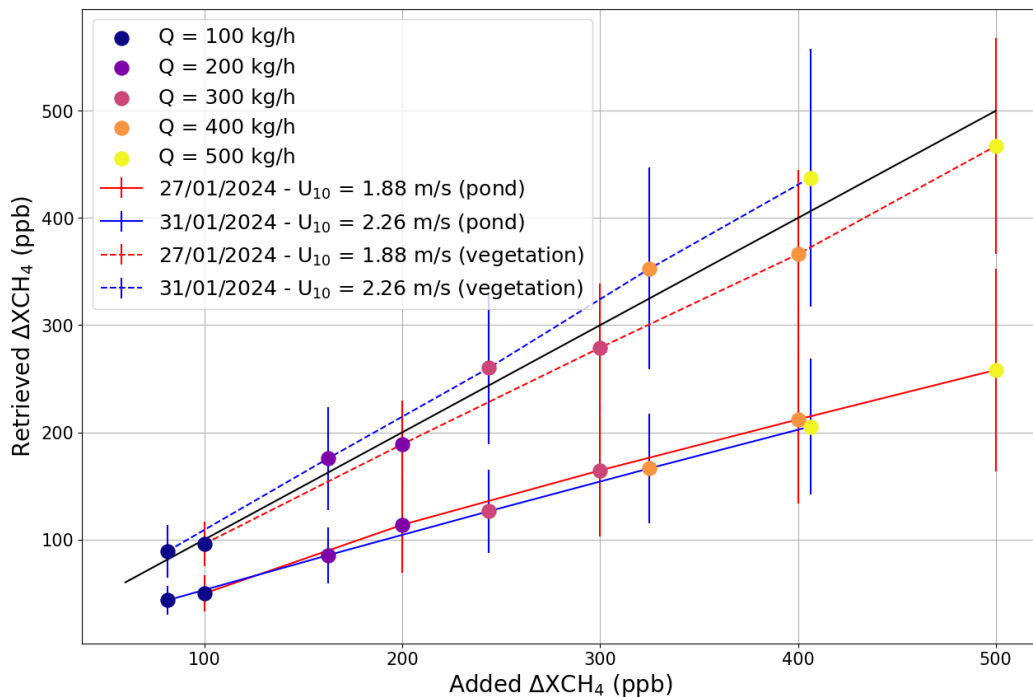
Figure S7. Scatter plot showing the relationship between the artificially added and retrieved enhancements over the pond pixels (solid lines) and over close-to-the-pond pixels covered by vegetation (dashed lines) on the EnMAP acquisitions on 27th (red) and 31st (blue) January. The added enhancement values are related to the mean maximum enhancement values from a subset of WRF-LES plumes associated with similar U10 values from each acquisition and to flux rate values ranging from 100 kg/h to 500 kg/h.